ARTICLE

Rationalising the Multivariate Modulation of MUV-10 for the Defect-Introduction of Multiple Functionalised Modulators

Received 00th January 2022,
Accepted 00th January 2022

DOI: 10.1039/x0xx00000x

Isabel Abánades Lázaro *[a]

Among multivariate Metal-Organic Frameworks, multivariate modulated (MTVM) MOFs offer the possibility of introducing multiple functionalised units into the MOFs as defect-compensating ligands promoting porosity among other defect-related properties. However, there are no studies that rationalise the incorporation of multiple functionalised modulators and their resultant properties, hindering their molecular design and multi-applicability. In this manuscript, we introduce up to five functionalised modulators bearing NO_2, F, tBu, OH and NH_2 units in significant quantities (up to *ca*. 31 mol%) into the Ti heterometallic MOF MUV-10 in one-pot synthesis, increasing the porosity up to *ca*. 1.3-fold in comparison with the pristine material. We have rationalised the incorporation ratios of the different combinations of modulators among other properties. As a proof-of-concept, we have shown that there is up to a 1.7-fold enhancement in the catalytic activity of MTVM MOFs for the regioselective opening of epoxides, anticipating that this protocol can be used to produce multi-functionalised materials with a wide range of applications.

Introduction

Multivariate Metal-Organic Frameworks (MTV MOFs) [1–4]– hybrid tridimensional porous networks formed of multiple metals and/or linkers in one phase – have properties unachievable in single-component phases [2,5] and are promising materials for environmental and healthcare applications. [2–8] However, the universal synthetic control of MTV MOFs is still a challenge that comes from the lack of interrelation between synthetic variables and MOF properties.

MTV MOFs were first reported in 2010 upon the addition of up to eight linkers to MOF syntheses, [2] demonstrating gas separation properties unobtainable for their separate phases. MTV MOFs with multiple linkers allow for the generation of porous materials with dual opposite properties in the same framework while tailoring the pore environment by the introduction of functional groups that enhance their application. However, a drawback in the multivariate linker approach is the often reduced porosity of the materials due to the introduction of functional groups. Although sequential linker installation and using linkers with different lengths have been used to control their incorporation ratio and position, [9–11] rationalisation on the incorporation ratio of functionalised linkers with similar lengths is still lacking.

Coordination modulation (CM) is a synthetic tool based on the introduction of ligands that compete with the multitopic linkers for metal complexation during MOF solvothermal synthesis, [12–14] and it is used to fine-tune MOF properties, such as crystallinity, [15] particle size, [16] defectivity [17,18] dispersity, [19] porosity, [20]chemical reactivity, [21] and stability [22]among others. Due to DMF decomposition to formic acid, coordination modulation occurs in any DMF containing synthesis. [20,23] However, the complex equilibria that govern their self-assembly are still not fully understood due to a lack of inter-relation between synthetic variables and properties. [12]

Among multifunctionalised frameworks, multivariate modulated MOFs (MTVM MOFs) were first reported in 2020, [5] with up to three different anticancer drugs simultaneously introduced as modulators during the Zr_6 MOF UiO-66 synthesis, resulting in high incorporation (up to 30% in weight) as defect compensating ligands of remarkably porous frameworks that allowed the loading of a fourth drug, resulting in MOFs loaded with a cocktail of drugs that had improved anticancer selectivity.

Despite the high potential of MTVM MOFs for many applications, offering the possibility of increasing the frameworks' porosity while including an array of functionalities into the frameworks' pores for selected applications, to the best of our knowledge there are no further examples in the literature. Thus, the lack of interrelation between the multiple modulator's functionalities, their incorporation into MTVM MOFs and the resultant properties hinders their molecular design and subsequent multi-applicability.

To this end, we have synthesized a set of MTVM MOFs containing up to 5 different functionalized modulators in the same frameworks as defect compensating ligands, rationalizing their properties such as preferred incorporation depending on

Instituto de Ciencia Molecular (ICMol)
Universitat de València,
Catedrático José Beltrán Martínez nº 2, 46980 Paterna, Valencia, Spain.
E-mail: Isabel.abanades@uv.es
Electronic Supplementary Information (ESI) containing experimental conditions and detailed caharacterisation available:

the attractive or repulsive interactions between modulators, resulting in up to a 1.35-fold increase in the materials surface area and 1.65-fold increase in their pore volumes. Moreover, we show that the multiple incorporation of modulators with functionalised cooperative units that enhances the diffusion of the substrates through the pore and their activation significantly enhances the catalytic performance of these materials for the regioselective transformation of pharmaceuticals of industrial relevance.

Results and Discussion

MUV-10, represented in **Figure 1a**, is a biocompatible 8,3-connected heterometallic Ti (IV)-MOF that is built of $Ti^{IV}_2Ca^{II}_2(\mu_3\text{-}O)_2(H_2O)_4(RCO_2)_8$ clusters connected by benzene tricarboxylate (BTC) linkers forming a cubic structure with the unit formula $[Ti_3Ca_3(\mu_3\text{-}O)_3(\mu_2\text{-}C_6H_3(CO_2)_3)_4(OH_2)_6]$. [24,25] This highly-stable (500°C) porous framework tolerates a high degree of defects (up to 40 molar%, 3 missing linkers out of 8 in the unit cell) while maintaining its thermal and chemical stability. [18] MUV-10 is amenable to defect promotion both through the addition of monocarboxylate and dicarboxylate modulators [18] and by depleting the linker to metal ratio during synthesis, [26] resulting in short-range correlated defect clusters that govern its pore size distribution.

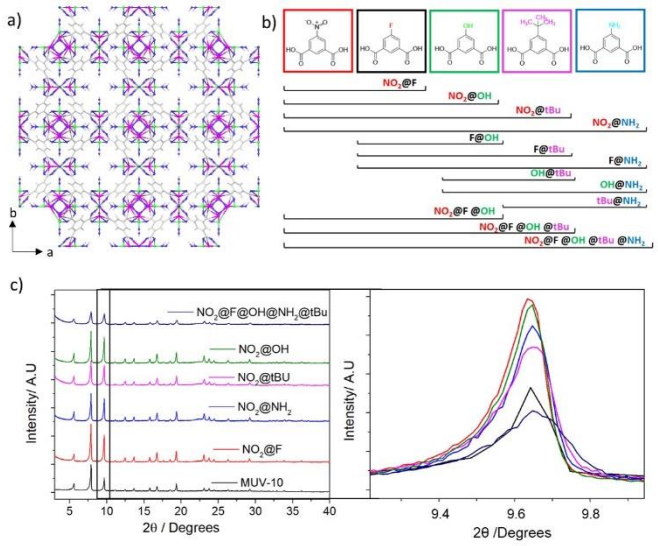

Figure 1: a) MUV-10 structure, b) array of MTVM MOF samples synthesised during this study and c) PXRD patterns of the NO_2@mod family and the penta-modulated MOF. Grey carbon atoms, white hydrogens, blue oxygens, green titanium and pink calcium.

We have selected 5-functionalised isophthalic acid modulators with either NO_2, F, OH, tBu and NH_2 units, shown in **Figure 1b**, which confer different acidity to the modulator with pK_a in the order NO_2 3.16 < F 3.23 < OH 3.32 < tBu 3.54 < NH_2 4.25, known to play an important role in modulators' incorporation. [19,20] Additionally, the modulators have different hydrophobicity tBu<NO_2<F<OH<NH_2 based on their partition coefficients (log P 1.895, 0.099, -0.002, -0.199, -0.61 respectively), and some of the functional groups shall allow for hydrogen-bond interactions, beneficial for catalysis and gas uptake/separation among other applications. [2,4,27–31]

To study the potential of the multivariate modulated protocols to introduce up to five functionalised modulators, and to rationalise the MOFs' properties based on the modulators introduced, we have synthesised a set of MTVM MOFs increasing complexity in tandem: first, the combination of 2 modulators, then three, four and finally five, as summarised in **Figure 1b.** We have labelled the di-modulated samples as mod1@mod, where mod1 corresponds to the common modulator in the series and mod to the variable modulator. Although in certain cases we have focused the discussion on different series or samples, full characterisation (PXRD, FT-IR, ^{1}HNMR, SEM, EDX, TGA, N_2 adsorption and desorption isotherms) is given in Section S.3 of the supporting information for all the samples.

During all the synthetic conditions we have used a fixed excess of linker (1.5 equivalents compared to metal), a synthesis that results in defect-free crystals [18,26] and thus allows us to study the effect on defectivity (among other variables) solely based on the modulators introduced. We have added one equivalent of each modulator in comparison to the linker (See S.2 for detailed synthetic conditions). Solutions containing the modulators together with the linkers and the metal salts were prepared and mixed once all the components were dissolved to avoid solubility-related variations that might influence the syntheses.

Rationalising the properties of MTVM MOFs

All the materials were highly crystalline and phase pure as envisioned in their highly-resolved PXRD profiles (**Figure 1c**), with Bragg diffraction bands confirming phase pure MUV-10, although minor shifting on the position of the signals was observed possibly as a consequence of structural distortion (See Figures S1-S10 in S3.1 for PXRD of all the samples). The materials displayed significant changes in the relative intensity of the peaks that suggests preferred incorporation in certain crystal regions, with a noticeable increase in relative intensity of the 111 reflection band, which corresponds to the perpendicular plane inside of the crystals, being approximately half the intensity of the 110 band in the unmodulated MOF and almost the same for the penta-modulated MOF as shown in **Figure 1c** and quantified in Figures S11 and S12. All the samples had Ti:Ca ratios according to the 1:1 cluster structure, as determined by Energy Disperse X-Ray, confirming together with PXRD profiles that there is no co-formation of a different Titanium or calcium phase, such as an oxide.

While acid-digested ^{1}HNMR showed high modulator's incorporation, as represented in **Figure 2a** (See S.3.2), FT-IR confirmed the modulators attachment, as no free carboxylate units were observed in any case, while the MOFs displayed profiles similar to pristine MUV-10, with characteristic vibration bands coming from the functionalized modulators, often masked by the MOF characteristic signals (See S.3.3).

The modulator' incorporation and total modulators incorporation into the multi-functionalised structures were

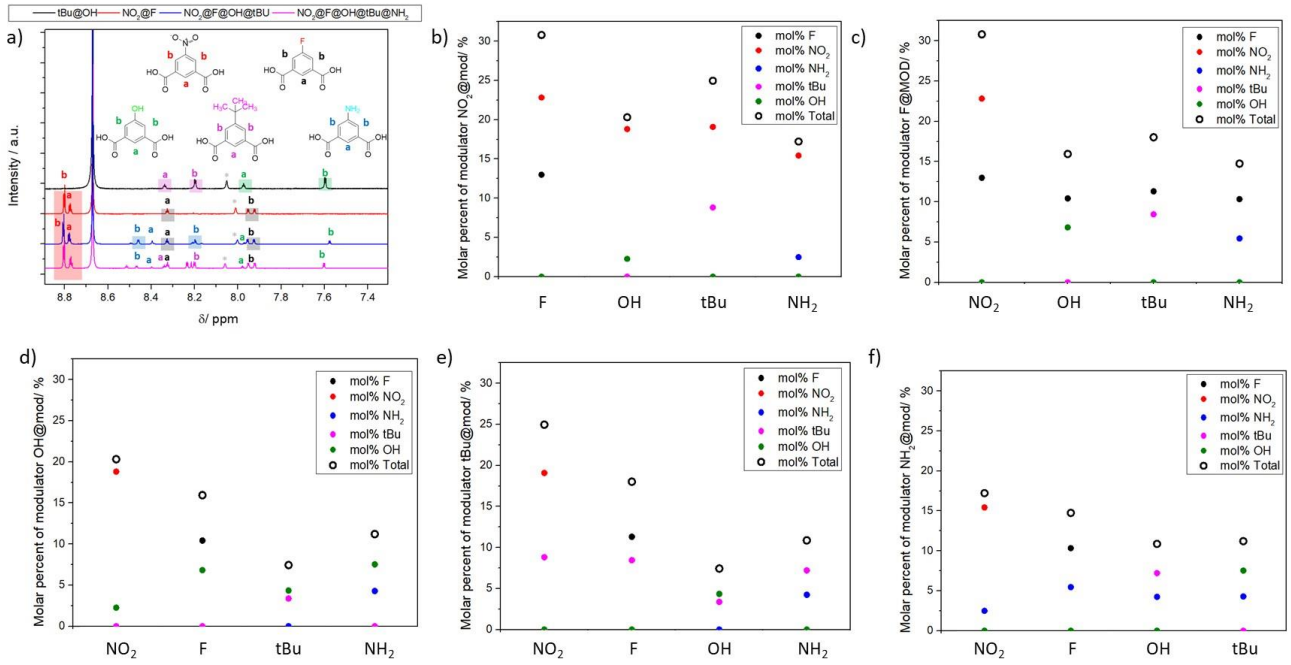

Figure 2:a) Representation of the ^{1}HNMR profiles of MTV MOFs showing the presence of multiple functionalised modulators. Representation of the modulators incorporation in molar percent into di-functionalised structures for b)NO_2@mof, c) F@MOD, d)OH@mod, e) tBu@mod and f) NH_2@mod.

calculated by ^{1}HNMR as molar% and molar ratio, ranging incorporation from *ca.* 7 to 31 mol% compared to the linker (See S.3.2 for a detailed explanation of the calculations). These incorporation degrees are remarkably high for the modulators to be only located at the MOF surfaces as capping ligands.[32] In general, the modulator's incorporation aligned with the modulator's acidity despite equimolar concentrations of modulators being present in the synthesis, which indicates different kinetic effects (See Figures S13-S27 in S.3.2 for ^{1}HNMR profiles and detailed analysis of all the samples). The highest incorporation for the di-modulated MOFs was for the combination of the most acidic NO_2- and F- functionalised modulators, (*ca.* 30 molar% of total modulator, *ca.* 23% NO_2 vs *ca.* 13% F), while the minor incorporation was for the combination of less acidic modulators tBu and OH (*ca.* 7 molar% of total modulators, *ca.* 4% OH vs *ca.* 3% tBu) and tBu and NH_2 modulators (*ca.* 11 % total modulators, *ca.* 7% tBu *vs ca* 4% NH_2). In all the series, the highest incorporation is for the most acidic modulator (NO_2) followed by F (second most acidic), and the incorporation ranges across the di-modulated series for the principal modulator agrees to its acidity.

However, to understand the trends in incorporation one has to envision the coordination modulation equilibria as a competition between linkers and modulators for metal complexation sites, where the deprotonation of the organic ligands, which is related to their acidity, plays an important role.[12,16] The more acidic the ligand, the higher its deprotonation and the higher the inhibition of the deprotonation of less acidic species.[16] Thus, more acidic modulators preferably coordinate to metal ions during MOF formation**.** [20] However, when adding multiple modulators attraction (i.e. H-bonding) and repulsion (i.e. different hydrophobic and hydrophilic modulators) effects between modulators should also be considered.

Differences in incorporation that cannot be attributed to the modulators' acidity are beautifully exemplified when we analyse the modulator incorporation to the di-modulated MOFs in series, as illustrated in **Figure 2**. In **Figure 2b** we observe that while for the NO_2@mod MOFs the NO_2 modulator (most acidic) incorporation into the framework (23-15 mol%) is slightly higher for the NO_2@F MOF, similar for OH and tBu co-modulation and lower upon the combination with NH_2, the incorporation of the second modulator decreases with the increase of their pK_a, apart from tBu, which incorporation is higher than OH despite the latter being more acidic. This is due to the similar hydrophobicity of tBu and NO_2 units that make their co-existence in the frameworks more attractive. Hence, the total amount of modulators is higher for the combination of NO_2 with hydrophobic F and tBu modulators than with hydrophilic OH and NH_2 modulators. A similar phenomenon is observed in the F@mod series represented in **Figure 2c**, with F incorporation (13-10 mol%) is slightly higher upon NO_2 and tBu co-modulation and where tBu incorporation is slightly higher than OH despite its lower acidity, leading to a higher mol% of total modulator incorporated for the combination of F with hydrophobic units (NO_2 and tBu).

The OH modulator has intermediate acidity, is hydrophilic and is well-known for its H-bond interactions with F and NH_2 groups. Thus, the OH modulator incorporation across the OH@mod series (8-2 mol%), represented in **Figure 2d**, is higher upon F and NH_2 co-modulation than upon tBu and NO_2 co-modulation, despite the differences in hydrophilicity between OH and F units and the different pK_a and hydrophilic nature of the F and NH_2

co-modulators. However, in this case, due to the high acidity of the hydrophobic NO_2 and F modulators, their incorporation is the most significant across the series, with a 19 and 10 mol% respectively. Among the tBu@mod series (9-3 mol%), represented in **Figure 2e**, tBu, which is the most hydrophobic modulator, incorporates less significant with OH (3%) co-modulation than upon F (8%) or NO_2 (9%) co-modulation, despite the last two being more acidic and providing both higher deprotonation inhibition and competition for metal-complexation. In contrast, while the incorporation of the NH_2 modulator in NH_2@mod MOFs (2-5mol%), represented in **Figure 2f,** is less significant in the presence of NO_2 modulator, the incorporation of the second modulator is related to their pK_a. The differences in the co-modulator incorporation compared with the other series could be due to the contrasting incorporation ratios which are in fact related to their distinct acidity. Thus, due to the low incorporation of NH_2 in comparison with other modulators, its role in the attraction/repulsion interactions is less significant.

Overall, these results show the importance of considering both the modulator's acidity, their hydrophobic/hydrophilic character, and the possible interactions between them such as hydrogen-bonding when designing an MTVM MOF. Importantly, these findings can also be extrapolated to MTV MOFs with multiple linkers bearing different functionalities, while we have not found examples in the literature that thoroughly cover the rationalisation of the incorporation ratios of multi-functionalised ligands with similar length.

The tri- tetra- and penta-functionalised structures incorporated a similar total percent of modulators (ca. 24-28 molar%), Figures S28 and S29, which is slightly smaller than for the NO_2@F MOF, indicating that multiple modulators with different hydrophobicity competing for the metal-complexation sites slightly reduces their incorporation. As more modulators are introduced to the synthesis, the NO_2 mol% decreases from 20 to 16 mol%, and similarly occurs for the F modulator that decreases from 10 to 8 mol%. However, this decrease is compensated by the incorporation of new modulators. NO_2@F@OH and NO_2@F@OH@NH_2 have modulators incorporated in agreement with their pK_a, while in NO_2@F@OH@NH_2@tBu, the tBu unit incorporated more significant than the OH modulator despite the lower acidity of the first. This is likely to be due to the highest incorporation of the most acidic modulators NO_2 and F that are as well the most hydrophobic and favour the incorporation of tBu over OH.

Under these synthetic conditions with the absence of isophthalic acid modulation, the **crystal size** is ~2 µm. However, upon the introduction of multiple functionalised modulators the particle sizes are reduced down to 600-100 nm for the di-modulated MOFs (depending on the modulators) and down to 112±33, 89±20 and 50±17 nm for the tri-, tetra- and penta-functionalised MOF respectively, as shown in **Table 1** and illustrated in **Figure 3a**, indicating a capping effect or a significant reduction in deprotonated linker concentration[16] (See S.3.4 for SEM images and statistical analysis of all MOFs).

Changes in morphology are also observed from octahedral crystals to round nanoparticles. Interestingly, among all the series, the MOF containing OH-functionalised modulator displays the biggest particle sizes, indicating different coordinating effects. Among the OH series, the samples display similar particle sizes within error (*ca.* 500-600 nm), apart from OH@NO_2 – for which OH content decrease in comparison to the rest of the series - with a particle size of 259±37 nm. Another peculiarity of the OH@mod series is that all the samples display a bright yellow colour, while the unmodulated MOF, and MTVM MOFs that do not contain OH modulator, are white. This indicates that the OH functionality might be participating in ligand-to-metal charge transfer or that it might be coordinating to the Ti/Ca positions or/and forming H-bonds with the axial waters of the clusters. [32] Apart from OH-containing MOFs, the particle size of the di-modulated MOFs is related to the modulators pK_a. The NO_2@mod series maintains a particle size of ca. 150±35 nm, suggesting that particle size is controlled by the NO_2 modulator. The F@tBu and F@NH_2 MOFs have particle sizes of ca. 315±150 nm, while F@NO_2 particles are 149 ±35 nm. Similarly, tBu@NH_2 particles measure 366 ±91 nm, while tBu@NO_2 114 ± 25 nm. This suggests that across each series NO_2 modulator decreases particle size due to its higher acidity that results in a higher capping effect due to the higher inhibition of linker deprotonation and its higher metal-complexation tendency.[16] Energy-dispersed X-Ray mapping (See S.3.4.B, Figures S46-54) confirmed the presence of the modulators' signature elements and their homogenous distribution.

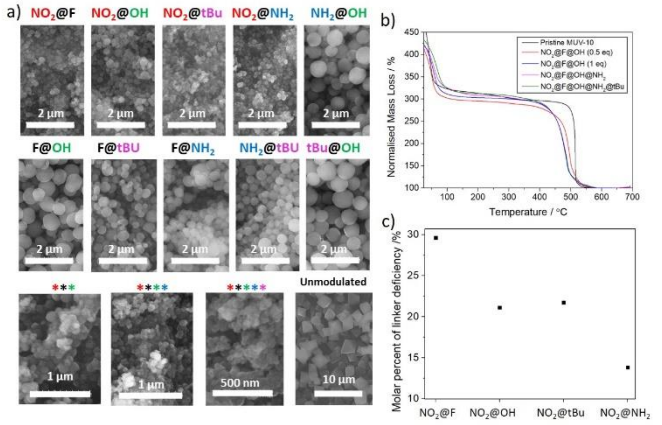

Figure 3: a) SEM images of the MTVM MOFs, b) Thermal decomposition profiles of the tri, tetra and penta-modulated MOFs and c) representation of the molar % of linker deficiency in the NO_2@mod series.

Thermogravimetric analysis showed the high thermal stability of the materials (400-500 °C), as shown in **Figure 3b.** We used TGA models [33] to analyse the composition of the materials, as well as their defective nature. It is important to remark that

Table 1: Tabulated data of particle size, molar percent of missing linkers, the linker to metal ratio, modulator per missing linker, BET surface area, micropore surface area, external surface area, micropore volume, mesopore volume and total pore volume.

Sample	Size ± SD	ML%	L:M	Mod/ML	S_{BET}	S_{MICRO}	S_{EXT}	V_{MICRO}	V_{MESO}	V_{TOTAL}
Pristine	2970±1215	0	1.40	0.00	1040	974	66	0.365	0.037	0.402
NO_2@F	149±35	29.6	0.94	1.06	1249	1050	199	0.411	0.166	0.577
NO_2@OH	259±37	21.1	1.05	0.95	1123	927	196	0.36	0.155	0.515
NO_2@tBu	114±25	21.8	1.04	1.20	1168	893	275	0.35	0.295	0.645
NO_2@NH_2	147±33	13.8	1.15	1.30	1124	976	148	0.375	0.088	0.463
F@OH	550±138	34.1	0.88	0.37	1164	1015	149	0.392	0.096	0.488
F@tBu	316±147	17.9	1.09	1.01	736	591	145	0.234	0.094	0.328
F@NH_2	312±81	14.4	1.14	1.03	1314	1142	172	0.443	0.109	0.552
tBu@OH	624±109	16.6	1.11	0.40	518	436	82	0.169	0.052	0.221
NH_2@OH	524±129	12.0	1.17	0.92	1116	994	122	0.378	0.076	0.454
NH_2@tBu	366±91	11.6	1.18	0.93	1030	834	196	0.324	0.156	0.48
F@NO_2@OH (0.5)	225±75	21.4	1.05	0.74	1080	857	223	0.336	0.194	0.53
F@NO_2@OH (1)	112±33	23.5	1.02	1.25	1164	932	232	0.364	0.194	0.558
F@NO_2@OH@NH_2	89±20	22.8	1.03	1.09	1206	932	274	0.366	0.072	0.438
F@NO_2@OH@NH_2@tBu	48±17	24.9	1.00	1.18	1148	835	313	0.333	0.319	0.652

ML%= molar percent of linker deficiency; L:M = linker to metal ratio; Mod/ML=modulator per linker defficiency; S_{BET} = Brunauer–Emmett–Teller surface area; S_{micro} = micropore surface area; S_{ext} = external surface area;V_{micro} = micropore volume; V_{meso} =mesopore volume; V_{total} = total pore volume.; Particle size is given in nm; Surface areas are given in m^2g^{-1} while pore volumes are given in cm^3g^{-1}.

although TGA is a valuable tool to characterise MOFs' composition it does not provide information about the type of defects and their distribution in the framework. During this discussion we have provided missing linker molar percent values in **Table 1,** which give more visual information about the linker deficiency in the frameworks, alongside the linker to metal ratio values, which can be used to calculate either the number of missing linkers or clusters in theoretical structures.

Surprisingly, the most defective sample, F@OH (*ca*. 35 molar percent missing linker, *ca.* 2.75 missing linkers out of 8) is not the one bearing the highest modulator incorporation but corresponds to the modulators with the highest H-bond interaction. This degree of defects is in tune with the maximum amount of defects reached by our previous study in single-modulated materials. [18] The second most defected material (F@NO_2) had a *ca*. 30% of missing linkers in the structure (2.4 missing linkers out of 8) and corresponds to the most acidic modulators that resulted in the highest modulators' incorporation. In general, one modulator (or combination of modulators) replaces one missing linker, as shown in **Table 1**, and the missing coordination position is compensated by OH / H_2O pairs (See S.3.5 for detailed models and composition of all materials). In the NO_2@mod series the defectivy of the materials (ranging *ca.* 30-14 mol% of missing linkers; 2.4-1.1 missing linkers out of 8), represented in **Figure 3c**, agrees with the incorporation tendencies previously discussed. In the F@mod series, F@OH is the most defective material and the only one where the missing linker defects are not fully compensated by modulators (*ca.* 0.37 modulator per missing linker), agreeing with the differences found in particle size. Apart from this sample, the defective nature of the series is in tune with the total % of modulators incorporated. In the OH@mod series, OH@F is the most defective sample, possibly due to the highest H-bond between modulators. The rest of the series agrees with the modulator's pK_a with one missing linker compensated by one modulator. The defectivity in the tBu@MOD series (21-11 molar% of missing linkers) is in great agreement with the modulator's pK_a, although again the tBu@OH sample is the only one in which missing linker defects are not fully compensated by modulators (0.4 modulators per missing linker), possibly due to the repulsion between hydrophobic tBu and hydrophilic OH units. NH_2@MOD series ranges 14-11 mol% of missing linkers in agreement with the modulator's acidity.

The tri- tetra- and penta-modulated MOFs have defectivity ranging 21-25 mol% (1.8-2 missing linkers out of 8), slightly increasing in agreement with incorporation. Across all the samples, each missing linker is compensated by modulators (ca. 1-1.2 modulators per missing linker) and the vacant coordination position is compensated by OH/H_2O pairs. This degree of defects is slightly smaller than upon certain di-modulated MOFs such as F@OH or F@NO_2, which points out, together with the incorporation trends, that having multiple modulators with repulsive interactions during synthesis can result in an overall decrease in incorporation compared to di-modulated MOFs in which both modulators have attractive interactions.

MUV-10 is a microporous framework, with a surface area of close to 1000 m^2g^{-1}, a pore volume of ca. 0.40 cm^3g^{-1} and a micropore of *ca.* 1 nm.[24] N_2 adsorption and desorption isotherms revealed the MOFs to be highly porous (S_{BET} 1150-1314 m^2g^{-1}), with the only exception of tBu@F and tBu@OH

which displayed a decrease in porosity in comparison with the pristine material (S_{BET} *ca.* 730 and 520 m^2g^{-1} respectively), possibly due to the bulkiness and higher molecular weight of the tBu modulator. The BET, microporous and external surface areas, alongside the micro, meso and total pore volumes are summarised in **Table 1.** The general increase in porosity arises from the modulators being introduced at defect sites and contrast with the MTV protocol to introduce multiple functionalised linkers in which the porosity typically decreases. The di-modulated materials conserve their type I isotherm, as shown in **Figure 4a** for the NO_2@mod family, although with higher uptake values despite some modulators weighting more than the linker and the values expressed per gram of material. This accounts for their structural integrity towards the incorporation of defect-compensating modulators. Among the NO_2@mod series **(Figure 4a and 4b)**, the most porous sample is NO_2@F, with *ca.* 1250 cm^3g^{-1} S_{BET} and a pore volume of 0.577 cm^3g^{-1}, while the rest of the series have similar S_{BET} (*ca.* 1125m^2g^{-1}) that slightly varies according to the modulators incorporation previously discussed. However, this is not the trend in all the series. Among the F@mod series, F@NH_2 is the most porous sample (S_{BET}=1314 m^2g^{-1}) followed by F@NO_2 (S_{BET}=1249 m^2g^{-1}) and F@OH (S_{BET}=1164 m^2g^{-1}). Among the OH@mod series all the samples, apart from tBu, have surface areas of *ca.* 1100 m^2g^{-1}. The tBu@mod series has reduced microporosity possibly due to the bulky character of tBu unit occupying pore space, whereas the NH_2@mod displays high porosity with NH_2@F being the most porous material (See S.3.6 supporting information for the analysis of each series).

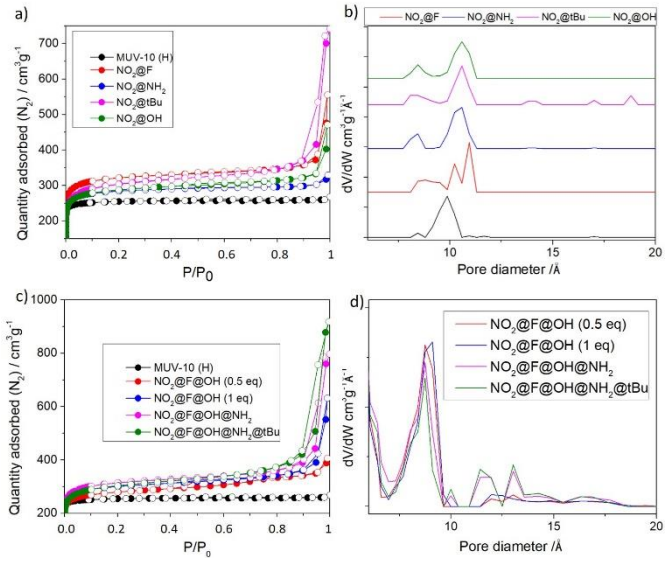

Figure 4: Porosity of multi-functionalised materials. a)N_2 adsorption and desorption isotherms of the NO_2@mod series, b) pore size distribution of the NO_2@mod series, c) N_2 adsorption and desorption isotherms of the tri, tetra and penta-functionalised MOFs and d) pore size distribution of the tri, tetra and penta-functionalised MOFs.

The increase in porosity was noticeable in their pore volumes, reaching up to ca. 0.65 cm^3g^{-1} at P/P_0 of 0.9, while the pristine material displays pore volumes of ca. 0.4 cm^3g^{-1}. Changes in the pore size distribution were apparent, with the formation of pores of bigger size (12 Å). While missing linker defects do not contribute to the formation of bigger pores in this framework, missing cluster defects lead to the appearance of a new pore at *ca.* 12 Å, in consonance with the PSD of these MTVM frameworks. [26] In the case of the multi-functionalized samples containing tBu units there is also the presence of a set of bigger pores of *ca.* 14 Å, 17 Å and 19 Å, which could be a consequence of the formation of missing clusters in close proximity due to its bulky character preventing the incorporation of linkers nearby. It is also possible that nano regions of missing clusters have a negative impact on the tBu@mod series microporosity. [3,8,35] Both the isotherm shape and PSD distribution change significantly upon the introduction of three or more functionalised modulators (**Figure 4c and 4d**) which is also envisioned in the pore fitting mismatch of the previous models. For these samples, type I isotherms shift into IV type isotherms with broader pores of bigger sizes (~2 nm) that suggests nanoregions rich in missing cluster defects and even bigger pores arising from inter-particle space (~25 nm).

Multivariate Modulation as a tool to tune the materials' catalytic properties

Introducing multiple functional units into the same framework is known to enhance applicability in different areas such as catalysis, photocatalysis or gas uptake among others. [3,6,8,36] Thus, as a proof-of-concept we have studied the potential of these multi-funcionalied MOFs for the straightforward synthesis of β-amino alcohols through regioselective ring-opening of oxiranes (epoxides) with amines, represented in **Figure 5,** at room temperature in EtOH (See S.5 in the supporting information for detailed conditions). As this reaction uses hydrophobic substrates while the epoxide substrate is activated through hydrogen bonding with OH and NH_2 units [37,38] we have studied the potential of MTVM MOFs bearing hydrophobic units or the combination of hydrophobic with OH and/or NH_2 moieties, summarised in **Table 2.** The results show that while the pristine material has a moderate conversion after 72 hours (*ca*. 44%), the most catalytically active material is the most hydrophobic NO_2@tBu (*ca.* 76%), which is followed by the penta-modulated material bearing all the functional units. F@NO_2 and F@tBu, also highly hydrophobic materials, but NO_2@OH and tBu@NH_2 have a higher performance. These results also show that the activity is not directly related to the materials' defectivity, for instance, NO_2@F has a ca. 30% linker deficiency, while NO_2@tBu has a ca. 23% of its linkers missing, and neither is related to particle size or porosity, as shown in Figures S95-98.

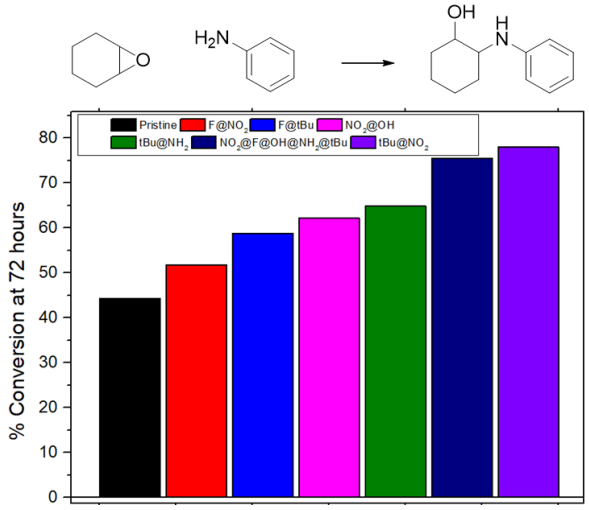

Figure 5: Catalytic conversion of MTVM MOFs at 72 hours for the regioselective ring-opening of cyclohexane oxide with aniline.

Table 2: Tabulated data of catalytic conversion.

Time	Pristine	F/ NO_2	F/ tBu	NO_2/ OH	tBu/ NH_2	penta	tBu /NO_2
0	0.0	0.0	0.0	0.0	0.0	0.0	0.0
12	5.6	7.4	6.0	13.4	10.8	11.1	11.3
24	13.5	18.6	26.3	23.9	22.3	28.8	38.0
48	11.7	34.3	37.3	38.4	53.1	62.7	62.4
72	44.3	51.8	58.8	62.1	64.8	75.6	78.0

Thus, while the most hydrophobic material is the most catalytically active, possibly due to the higher diffusion of the reactant through the pore, the trends in conversion are followed by the materials that combine the most hydrophobic units (i.e. tBu or NO_2) with functionalities that activate the epoxide substrate through hydrogen bonding, such as NH_2 and OH. [37,38]

Although we have used catalytic testing as a proof-of-concept of the potential of the MTVM protocol to tune catalytic performance, and thus catalytic cycles and recycling are out of the scope of this study, PXRD patterns of the MOFs after 72 h of reaction (Figures S88-94) indicate, together with modulators or linker not being present in the gas chromatography analysis, structural integrity of the samples during the catalytic reaction.

Conclusions

These results account for the high potential of the multivariate modulation protocol to synthesise multi-functionalised structures containing up to five functionalised modulators with up to a *ca.* 31 molar% of incorporation compared to the linker as defect-compensating ligands, while significantly increasing the material's porosity (up to 1.35-fold increase in surface area and 1.65-fold increase in pore volume).

The rationalisation of the incorporation ratio shows the importance of taking into account both the modulators' acidity and the attraction/repulsion interactions between the multiple modulators when designing a multivariate modulated MOF. Although the modulator's acidity governs which modulator will be preferably incorporated, the interaction between modulators play an important role in their incorporation, and when both modulators are highly acidic, the incorporation ratio across the series is more influenced by their interaction than by their relative acidity, with the combination of hydrophobic or hydrophilic modulators resulting in higher incorporation than the mix of them. Additionally, it has been shown that hydrogen bonding is also an important factor to overcome the repulsion between hydrophobic and hydrophilic modulators. Importantly, these findings can be extrapolated to multivariate MOFs with multiple linkers.

As a proof-of-concept of the potential of multi-functionalised MOFs with the MTVM protocol to increase their application we have studied their catalytic activity for the regioselective ring-opening of epoxides with amines, showing that while the MOFs' defectivity, particle size and porosity are not related to the materials' performance, the functionalities introduced are fundamental factors. Being the reaction substrates hydrophobic, the most active material is the one bearing the most hydrophobic units, enhancing the diffusion of the substrate to the pore. As the epoxide is activated through hydrogen bonding with NH_2 and OH moieties, the trends in catalytic activity are followed by materials that combine hydrophobic units with these functionalities.

Overall, we have shown the versatility of the MTVM protocol to introduce up to five functional units in significant quantities into the framework, we have rationalised incorporation trends that shall bring light into the design of multi-functionalised MOF structures while increasing their porosity and we have proven the potential of this protocol to increase the application of MOFs.

Conflicts of interest

There are no conflicts to declare.

Acknowledgements

This work was supported by the Horizon 2020 research and innovation programme under the Marie Skłodowska grant agreement No 837804 (DefTiMOFs, MSCA-IF-2018). I.A.L thanks the European Union's Horizon 2020 research and innovation programme for the receipt of MSCA Individual Fellowship, MINECO for a Juan de la Cierva Incorporacion Fellowship (IJC2020-044374-I) and The University of Valencia for research facilities. Enrique Navarro Raga is acknowledged for assistance with EDX mapping and Francisco Garcia Cirujano for meaningful discussion regarding catalytic testing.

Notes and references

1 Z. Ji, T. Li, O. M. Yaghi, *Science* 2020, **369,** 674–680.
2 H. Deng, C. J. Doonan, H. Furukawa, R. B. Ferreira, J. Towne, C. B. Knobler, B. Wang, O. M. Yaghi, *Science* 2010, **327**, 846.

3 A. Helal, Z. H. Yamani, K. E. Cordova, O. M. Yaghi, *Natl. Sci. Rev.* 2017, **4**, 296.
4 J. Jiao, W. Gong, X. Wu, S. Yang, Y. Cui, *Coordin. Chem. Rev.* 2019, **385**, 174.
5 a) I. A. Lázaro, C. J. R. Wells, R. S. Forgan, *Angewandte Chemie In.t Ed.* 2020, **59**, 5211.b) I. A. Lázaro, C. J. R. Wells, R. S. Forgan, *Angewandte Chemie*, 2020*,* **132***,* 5249.
6 M. Mon, R. Bruno, E. Tiburcio, M. Viciano-Chumillas, L. H. G. Kalinke, J. Ferrando-Soria, D. Armentano, E. Pardo, *J. Am. Chem. Soc.* 2019, **141**, 13601.
7 S. Li, Y. G. Chung, C. M. Simon, R. Q. Snurr, *J. Phys. Chem. Lett.* 2017, **8**, 6135.
8 H. Furukawa, K. E. Cordova, M. O'Keeffe, O. M. Yaghi, *Science* 2013, **341**, 1230444.
9 S. Yuan, W. Lu, Y.-P. Chen, Q. Zhang, T.-F. Liu, D. Feng, X. Wang, J. Qin, H.-C. Zhou, *J. Am. Chem. Soc.* 2015, **137**, 3177
10 Q. Pang, B. Tu, Q. Li, *Dalton. T.* 2019, **48**, 12000.
11 S. Yuan, Y.-P. Chen, J.-S. Qin, W. Lu, L. Zou, Q. Zhang, X. Wang, X. Sun, H.-C. Zhou, *J. Am. Chem. Soc.* 2016, **138**, 8912.
12 R. S. Forgan, *Chem. Sci.* 2020, **11**, 4546.
13 H. Guo, Y. Zhu, S. Wang, S. Su, L. Zhou, H. Zhang, *Chem. Mater.* 2012, **24**, 444.
14 S. Griffin, M. Briuglia, J. ter Horst, R. S. Forgan, *Chem - European J.* 2020, **26**, 6910.
15 R. J. Marshall, C. L. Hobday, C. F. Murphie, S. L. Griffin, C. A. Morrison, S. A. Moggach, R. S. Forgan, *J. Mater. Chem. A.* 2016, **4**, 6955.
16 C. R. Marshall, S. A. Staudhammer, C. K. Brozek, *Chem. Sci.* 2019, **10**, 9396.
17 K. Tan, H. Pandey, H. Wang, E. Velasco, K.-Y. Wang, H.-C. Zhou, J. Li, T. Thonhauser, *J. Am. Chem. Soc.* 2021, **143**, 6328.
18 I. A. Lázaro, N. Almora-Barrios, S. Tatay, C. Martí-Gastaldo, *Chem. Sci.* 2020, **12**, 2586.
19 W. Morris, S. Wang, D. Cho, E. Auyeung, P. Li, O. K. Farha, C. A. Mirkin, *ACS Appl. Mater. Inter.* 2017**, 9**, 33413.
20 G. C. Shearer, S. Chavan, S. Bordiga, S. Svelle, U. Olsbye, K. P. Lillerud, *Chem. Mater.* 2016, **28**, 3749.
21 O. V. Gutov, M. G. Hevia, E. C. Escudero-Adán, A. Shafir, *Inorg. Chem.* 2015, **54**, 8396.
22 B. V. de Voorde, I. Stassen, B. Bueken, F. Vermoortele, D. D. Vos, R. Ameloot, J.-C. Tan, T. D. Bennett, *J. Mater. Chem. A.* 2014, **3**, 1737.
23 C. Atzori, G. C. Shearer, L. Maschio, B. Civalleri, F. Bonino, C. Lamberti, S. Svelle, K. P. Lillerud, S. Bordiga, *J. Phys. Chem. C.* 2017, **121**, 9312.
24 a) J. Castells-Gil, N. M. Padial, N. Almora-Barrios, J. Albero, A. R. Ruiz-Salvador, J. González-Platas, H. García, C. Martí-Gastaldo, *Angewandte Chemie. Int. Ed.* 2018, **57**, 8453. B) J. Castells-Gil, N. M. Padial, N. Almora-Barrios, J. Albero, A. R. Ruiz-Salvador, J. González-Platas, H. García, C. Martí-Gastaldo, *Angewandte Chemie* 2018, **130**, 8589.
25 I. A. Lázaro, J. M. Rodrigo-Muñoz, B. Sastre, M. R. Ángel, C. Martí-Gastaldo, V. del Pozo, *J. Mater. Chem. B.* 2021, **9**, 6144.
26 I. A. Lázaro, N. Almora-Barrios, S. Tatay, C. Popescu, C. Martí-Gastaldo, *Chem. Sci.* 2021, **12**, 11839.
27 S. A. A. Razavi, A. Morsali, *Coordin. Chem. Rev.* 2019, **399**, 213023.
28 A. U. Czaja, N. Trukhan, U. Müller, *Chem. Soc. Rev.* 2009, **38**, 1284.
29 T. Zhang, W. Lin, *Chem. Soc. Rev.* 2014, **43**, 5982.
30 J.-D. Xiao, H.-L. Jiang, *Accounts. Chem. Res.* 2019, **52**, 356.
31 M. J. Kalmutzki, C. S. Diercks, O. M. Yaghi, *Adv. Mater.* 2018, **30**, 1704304.
32 G. Oberdörster, E. Oberdörster, J. Oberdörster, Environ. Health Perspect., 2005, **113**,823.
33 J. Wang, A. S. Cherevan, C. Hannecart, S. Naghdi, S. P. Nandan, T. Gupta, D. Eder, *Appl. Catal. B. Environ.* 2021, **283,** 119626.
34 I. A. Lázaro, *Eur. J. Inorg. Chem.* 2020, **2020**, 4284.
35 W. Liang, C. J. Coghlan, F. Ragon, M. Rubio-Martinez, D. M. D'Alessandro, R. Babarao, *Dalton. T.* 2016, **45**, 4496.
36 Y. Wang, H. Lv, E. S. Grape, C. A. Gaggioli, A. Tayal, A. Dharanipragada, T. Willhammar, A. K. Inge, X. Zou, B. Liu, Z. Huang, *J. Am. Chem. Soc.* 2021, **143**, 6333.
37 P. Yingcharoen, W. Natongchai, A. Poater, V. D. Elia, *Catal. Sci. Technol.* 2020, **10**, 5544.
38 C. Claver, M. B. Yeamin, M. Reguero, A. M. Masdeu-Bultó, *Green Chem.* 2020, **22**, 7665.